CHAPTER 2: Materials and methods

2.1 Introduction

This chapter portrays the experimental and computational protocols in this thesis work. All the chemicals used are tabulated appropriately. The details of different characterization techniques have also been discussed. Moreover, the chapter also describes the general procedure followed for evaluating the photocatalytic activities of the doped-Ag_2O materials prepared in this thesis work.

2.2 Chemicals

All the chemicals were of analytical grade and utilized without further purification in all the synthesis. Table 2.1 tabulates the chemicals used in this thesis. Deionized double distilled water (DDDW) was the synthesis medium. The photocatalytic performances of prepared materials were also evaluated in the same medium.

Table 2.1 Details of chemicals used in this thesis

SL No	Chemical name	Formula	Molecular mass (mole/g)	Physical appearance	Manufacturer
1	Silver nitrate	$AgNO_3$	169.87	Colorless crystal	Merck
2	Zinc nitrate hexahydrate	$Zn(NO_3).6H_2O$	297.49	White crystalline salt	SRL Chem
3	Nickel nitrate	$Ni(NO_3)_2.6H_2O$	290.79	Green	Merck

	hexahydrate			crystal	
4	Thiourea	$CS(NH_2)_2$	76.12	Colorless crystal	Merck
5	Cadmium nitrate tetrahydrate	$Cd(NO_3)_2.4H_2O$	308.49	Colorless crystal	Merck
6	Bismuth nitrate pentahydrate	$Bi(NO_3)_3.5H_2O$	485.07	Colorless crystal	Merck
7	Ammonium metavanadate	NH_4VO_3	116.98	White powder	HIMEDIA
8	Sodium hydroxide	NaOH	40.00	Solid pellet	Merck
9	Nitric acid	HNO_3	63.01	Colorless liquid	Merck
10	Methyl orange	$C_{14}H_{14}N_3NaO_3S$	327.33	Orange powder	Molychem
11	Rhodamine B	$C_{18}H_{31}ClN_2O_3$	479.02	Green powder	Merck
12	Ciprofloxacin	$C_{17}H_{18}FN_3O_3.HCl$	367.82	White powder	HIMEDIA
13	Isopropyl alcohol	C_3H_8O	60.10	Colorless liquid	HIMEDIA
14	Potassium iodide	KI	166.00	White salt	SRL Chem
15	p-	$C_6H_4O_2$	108.09	Yellow	Sigma Aldrich

	Benzoquinone			crystal	
16	Hydrochloric acid	HCl	36.46	Colorless liquid	Merck

2.3 Sample preparation

All the materials were prepared by precipitation followed by a hydrothermal treatment method. A stainless steel autoclave was utilized for the hydrothermal treatment. Details of the sample preparation are given in the sample preparation sections of respective Chapters 3, 4, 5, and 6.

2.4 Materials characterization techniques

This section describes the techniques used to characterize the prepared photocatalysts. The X-ray diffraction (XRD) technique was applied to identify the phases present in the prepared solid materials. Further, the high-resolution XRD (HR-XRD) pattern probed the material's characteristic peak, indicating whether the dopant has occupied an interstitial position or substituted the corresponding cation or the anion. The UV-visible diffuse reflectance spectroscopy (UV-DRS) recorded the reflectance data of the synthesized samples. The Tauc plot derived from the UV-DRS data gave the photocatalyst’s bandgap. The transmission electron microscope (TEM) was used to capture the sizes and shapes of the prepared nanoparticles. High-resolution TEM (HR-TEM) imaging helped to photograph the crystalline fringes. The d-spacing between two fringes (also represents the lattice d-spacing) identified the presence of a particular phase. High-resolution scanning electron microscopy (HR-SEM) was also used to investigate the morphology of the prepared nanomaterials. Photoluminescence (PL) studies were performed to measure the fluorescence intensities of the solid samples. X-ray photoelectron spectroscopy (XPS) investigation was done to analyze the elements present, their oxidation states, and the defect present in the materials. It further gives the binding energies of the constituent elements. UV-visible spectroscopy was used for absorbance measurement of reaction mixtures subjected to photocatalytic degradation.

2.4.1 Powder X-Ray Diffraction (XRD)

XRD is a powerful technique for analyzing solid-state phases, crystallite sizes, etc. (Kedesdy & Drukalsky, 1954; Patterson, 1939). It also provides the crystalline structure of the nanoparticles (Mourdikoudis et al., 2018). It is a non-destructive process because the solid samples can be recovered after the analysis. Rigaku Miniflex 600 Desktop (RIGAKU Corporation, Japan) instrument was used to record all the powder XRD patterns. The instrument had a Cu Kα irradiation source ($\lambda = 1.54056$ Å). During the pattern collection, the scan rate and step size were 5^{o} per min and 0.01. The 2θ angle was maintained between 15^{o} and 85^{o}. Rigaku SmartLab 9kW Powder type (without χcradle) model (RIGAKU Corporation) produced HR-XRD. The XRD peaks were matched with standard XRD patterns (JCPDS database) to identify the phases formed. The lattice parameter was calculated with the help of the following Bragg's equation (Pope, 1997).

$$n\lambda = 2\mathrm{d}\sin\theta \qquad (2.1)$$

Where the order of reflection is assigned as n, λ is the wavelength of incident X-ray radiation, and θ is the Bragg angle between the incident light and the crystallographic plane. Figure 2.1 depicts the whole process.

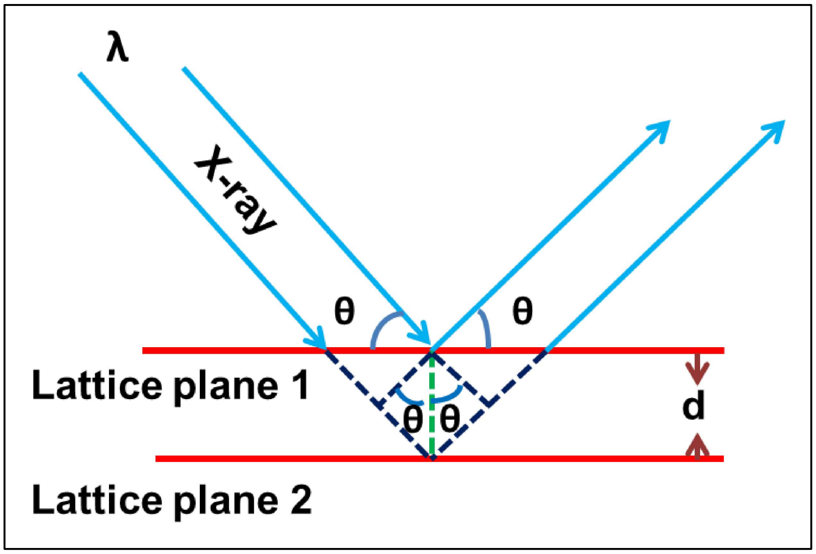

Figure 2.1 Schematic diagram of Bragg's diffraction law.

2.4.2 Transmission Electron Microscopy (TEM) sample preparation and imaging

TEM tool is very useful for nanoscale imaging. Further, the high-resolution images give the structural information of the specific crystalline phases (Smith, 2015). It can also analyze the nanoparticle shapes and sizes. This thesis utilized a standard method for TEM sample preparation. First, the nanoparticles (of the concerned sample) were dispersed in ethanol by proper sonication and dilution. Then, one drop of the re-dispersed sample was transferred to the TEM grid (Cu grid with 400 mesh size). The sample grid was dried in an oven at 50°C overnight. Tecnai G2 20 TWIN (EDAX Inc.) instrument (see Figure 2.2) using 200 kV accelerating voltage examined the prepared TEM sample grid. The images were collected from the different regions of the grid. The images give shapes and average particle sizes. The average particle sizes and fringes d-spacing were calculated using ImageJ software.

Figure 2.2 TEM instrument (Model: Tecnai G2 20 TWIN).

2.4.3 Scanning Electron Microscope (SEM) sample preparation and imaging

SEM imaging and Energy Dispersive Spectroscopy (EDS) were undertaken for nanoparticle imaging and analyzing the elemental composition of the samples. The samples were prepared following the standard sample protocol for powder nanoparticle samples. First, a small amount of powder sample was properly spread on carbon tape. The excess sample was removed by a small air duster. The prepared carbon tape was put in the SEM instrument for imaging. All SEM images were captured on the Nova Nano

SEM 450 (FEI Company of USA (SEA) PTE, LTD) instrument. EDS was recorded on Team Pegasus Integrated EDS-EBSD with Octane Plus and Hikari Pro (Company: EDAX Inc.). Figure 2.3 gives the combined set-up of the instrument.

Figure 2.3 FE-SEM instrument (model: Nano Nova SEM 450).

2.4.4 UV-Visible spectroscopy

UV-visible absorption spectroscopy is an analytical technique that measures light absorbance in the ultraviolet (UV) and visible regions of the electromagnetic spectrum. Light can be absorbed, transmitted, and reflected when it passes through the sample solution. Light absorption photo-excites electrons in a molecule by n- π*, π- π*, n- σ* (where the symbols indicate non-bonding orbital (n), bonding π-orbital (π), anti-bonding π–orbital (π*) or anti-bonding σ-orbital (σ*)) electronic excitations. The functional groups in the molecule cause a specific absorption, which is detected by a UV-vis detector and recorded as a UV-vis absorbance spectrum.

The Agilent Cary 60 spectrophotometer (the model shown in Figure 2.4) generates all UV-visible spectra of the samples. The diluted sample solution was taken in a cuvette of 1 cm path length and put in the spectrometer's sample holder slot. Note that the solvent was used for baseline correction.

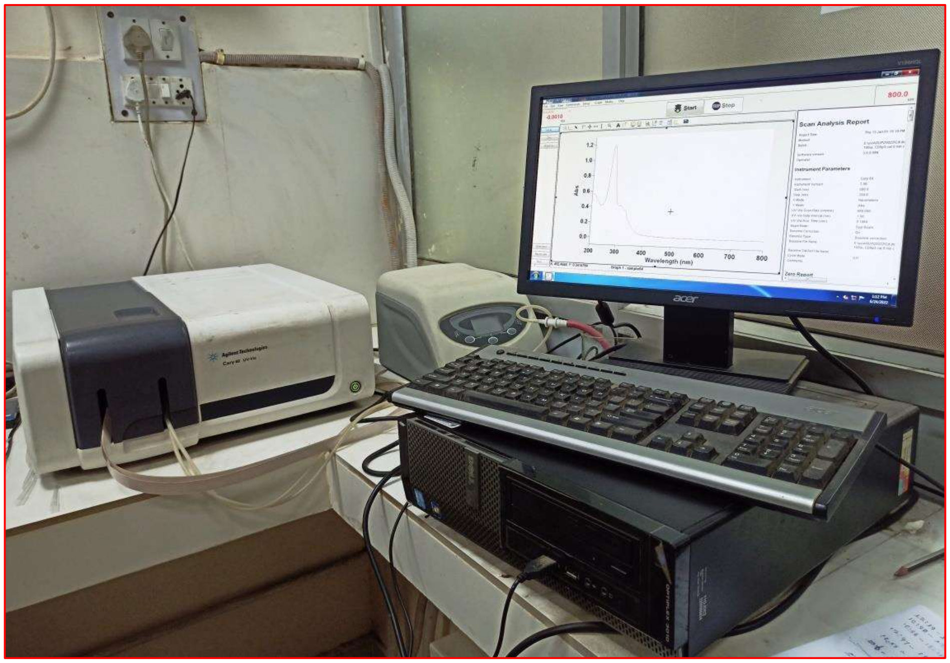

Figure 2.4 Agilent Cary 60 spectrophotometer.

2.4.5 UV-visible diffuse reflectance spectroscopy (UV- DRS)

The UV-DRS was utilized to measure the bandgap of the synthesized photocatalysts. The UV-2600 spectrophotometer (Figure 2.5) (Shimadzu Company) recorded the reflectance spectra of samples. Then, the absorbance data was acquired from the reflectance data using the Kubelka-Munk method (Molenaar et al., 1999; L. Yang & Kruse, 2004). The absorbance data generated the Tauc plots by the following relation (equation 2.3).

$$(\alpha h\upsilon)^{1/n} = (h\nu - E_g) \tag{2.3}$$

Here, α is the molar absorption coefficient, E_g and ν are the material's bandgap and frequency of light. The x-axis intercept of the tangent to the linear part of the plot ($(\alpha h\upsilon)^{1/n}$ vs. $h\upsilon$) gives the optical band gap (E_g) value of the photocatalyst. The n value governs the nature of the optical bandgap. For direct and indirect bandgap, the value of n is ½ and 2, respectively.

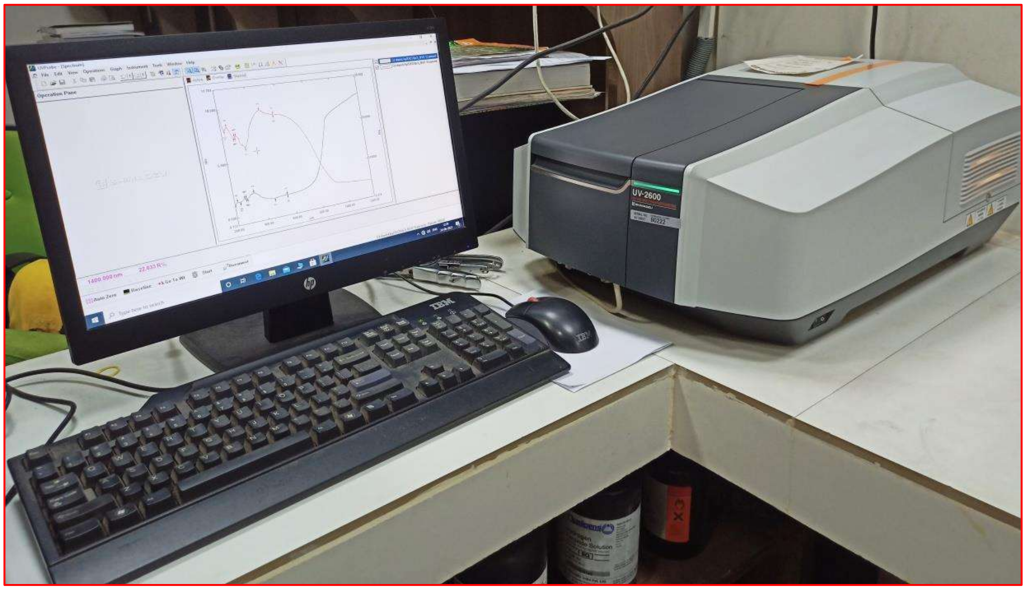

Figure 2.5 Shimadzu UV 2600 spectrophotometer.

2.4.6 X-ray photoelectron spectroscopy (XPS)

XPS is a quantitative analytical technique that measures the chemical state of the elements present in the material. When X-rays fall on the material, it causes the photoelectric effect. The ejected electrons move with certain kinetic energies that are analyzed by a detector. The binding energies are derived from these kinetic energies.

Notably, the binding energy of an element of a particular oxidation state is specific. Sample preparation for the XPS measurement followed a standard protocol. First, the powder sample was dispersed in ethanol and then dropped on a square-shaped small glass slide. The treated glass slide was then dried in a hot air oven. The glass slide with the sample thin film was subjected to XPS measurements. All the XPS measurements were carried out on the K-ALPHA XPS instrument (company: Thermo Fisher Scientific) (see Figure 2.6). Experimental data of the VB and CB positions are given with respect to the normal hydrogen electrode (NHE) scale (valence band XPS (VB-XPS)).

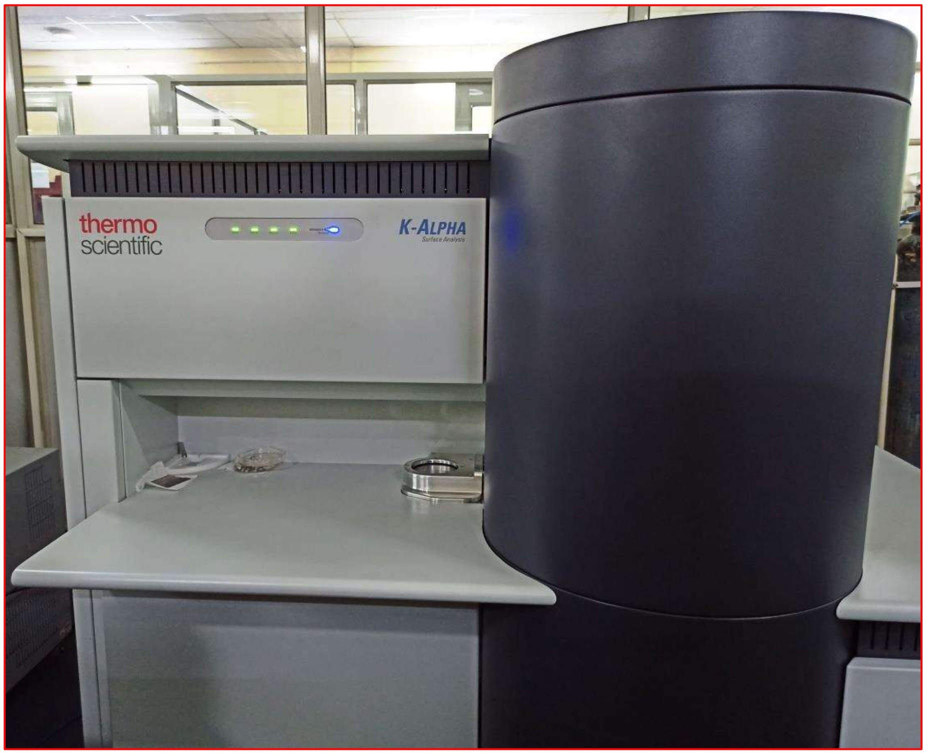

Figure 2.6 XPS instrument K-ALPHA model.

2.4.7 Spectrofluorimetry

The prepared samples' photoluminescence (fluorescence) (PL) was measured on two spectrofluorometers. The models used were the HORIBA PTI QM-400 and the

WITec alpha300 RAS spectrofluorometers. The fluorescence intensities of Zn and Ni-doped Ag_2O samples (Chapters 3 and 4) were measured on the HORIBA PTI QM-400 spectrofluorometer instrument. The WITec alpha300 RAS spectrofluorometer model was used to measure the fluorescence intensities of all the samples in Chapter 5. The aqueous dispersion of the samples was taken for the measurements in Chapter 3. Solid powder samples were directly used for measurements in Chapters 4 and 5.

2.5 Photocatalytic performance measurements

A homemade cube-shaped box inside one magnetic stirrer and bulb holder was used as a photocatalytic chamber. Figure 2.7 gives the outer and inner view of the photocatalytic chamber. A 14W Philips cool white LED bulb was taken as a visible light irradiation source. The intensity of the incident light was ~720 W/m^2, measured by a TM-206 power meter (pyranometer) device.

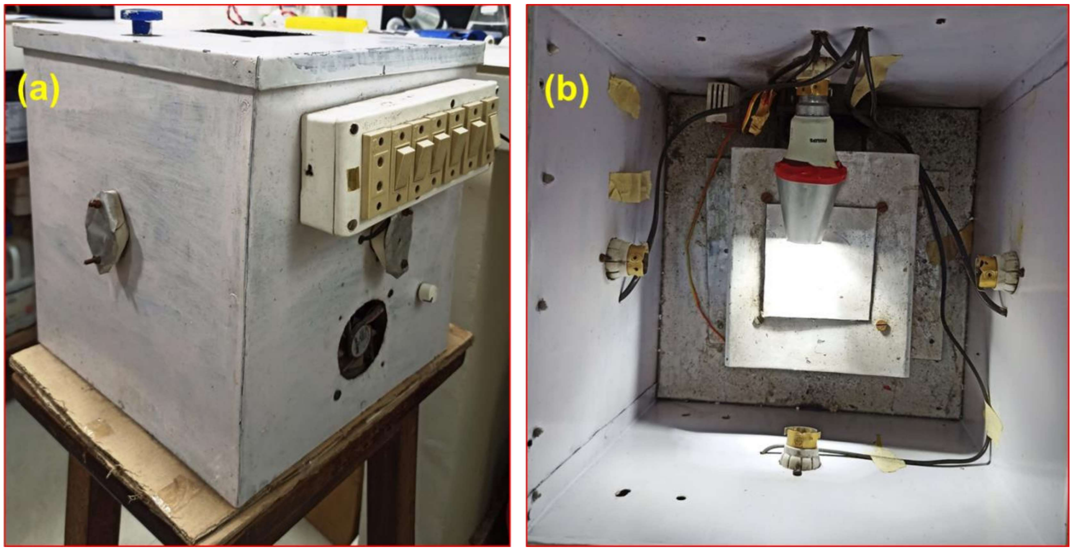

Figure 2.7 (a) Outer, and (b) inner view of the photocatalytic chamber.

The photocatalyst sample nanoparticles were re-dispersed in an appropriate volume of water on an ultrasonic bath. Then the re-dispersed sol was mixed with the organic molecule to be photocatalytically degraded in a 4 ml quartz cuvette. The resultant mixture was dispersed correctly using an ultrasonic bath. Then, the mixture was exposed to visible light irradiation. The UV-Visible absorption spectra were recorded after a specific time interval. The details of the photocatalytic experiments are separately given in Chapters 3, 4, 5, and 6. Turnover frequency (TOF) values of the catalysts were also calculated to determine the catalytic efficiency in a quantitative manner. The TOF determination experiment was similar to the photocatalytic experiments. All the TOF values in the thesis were calculated using the below equation (equation 2.4),

$$TOF = \frac{\left[\frac{Number\ of\ moles\ of\ reactant}{Number\ of\ grams\ of\ catalyst}\right] \times Yield}{time} \tag{2.4}$$

2.6 Electrochemical measurements

Electrochemical measurement data recorded on Metrohm Multi autolab/M204 instrument. First, the re-dispersed photocatalyst suspension was cast on the working electrode. Note that electrochemical measurements were performed for samples in Chapter 6. The Ag/AgCl (reference electrode), Pt (counter electrode), and glassy carbon (working electrode) electrodes were assembled in 0.5M Na_2SO_4 solution to measure electrochemical impedance. The impedance data were collected between -0.9V to +0.9V potential (at a fixed 0.005V amplitude and ~1 kHz frequency). Mott-Schottky plots and the CB position of the D1 photocatalyst were generated from the potential vs. NHE data graph. The latter was converted from the potential vs. Ag/AgCl electrode using the following relation (U. Kumar, Kuntail, et al., 2022; Lu et al., 2018),

V (NHE) = V (Ag/AgCl) + 0.059 pH+ 0.197 (here pH= 7)

2.7 Computational protocol

2.7.1 Plane-wave density functional theory (DFT)

DFT simulation with plane-wave basis sets is a powerful technique in semiconductor physics. It can generate various crystal and electronic structure information about semiconductor materials (Hasnip et al., 2014). The entire field of DFT is based on two fundamental theorems given by Kohn and Hohenberg and some derived equations by Kohn and Sham. Materials consist of many atoms. These atoms, in turn, consist of nuclei and many-electron wave functions. A nucleus has a larger mass than an electron. Therefore, the electronic wave function can be decoupled from the nuclear wave function due to the classical behavior of the nucleus (Born-Oppenheimer approximation). But, the electron-electron interactions require solving the many-body Schrodinger equation. The complexity of solving the many-body Schrodinger equation can be alleviated by DFT calculation. Because DFT only focuses on the electrons density instead of electrons wave functions. The electron density, $n(r)$ at a particular position in space is described by the following relation (equation 2.5) (Sholl & Steckel, 2009),

$$n(r) = 2 \sum_i \psi_i^*(r)\psi_i(r) \tag{2.5}$$

Here the symbol $\psi_i(r)$ is the individual electronic wave function, and the asterisk sign denotes a complex conjugate of the wave function. Here, the summation term is the probability of finding an electron at position r. Factor 2 appears due to two different spins of an electron.

The DFT calculations carried out in this thesis used generalized gradient approximations (GGA), and Perdew-Burke-Ernzerhoff (PBE) functional with projector augmented wave (PAW) pseudopotentials. GGA is an extension of the local density approximation (LDA), which can give exchange-correlation (XC) energy density. GGA methodically improves the atomization energy of the solid. There are other approximations over the GGA, i.e., (i) DFT + U (ii) meta-GGA (iii) hybrid functionals etc. (Hasnip et al., 2014; Hutchinson et al., 2016). Due to its low computational cost, the DFT calculations in this thesis were carried out only with GGA-PBE functional and PAW pseudopotentials.

2.7.2 Computational protocol

All the DFT calculations were performed on Medea molecular modeling software (version 1.0) interface using VASP (Vienna ab-initio simulation package) (VASP 5.4.4). The details models of the respective systems are discussed in Chapters 3, 4, 5, and 6.